Tuning and Switching the Hypersonic Phononic Properties of Elastic Impedance Contrast Nanocomposites

Akihiro Sato,[†,◆] Yan Pennec,[‡] Nitin Shingne,[§,⊥] Thomas Thurn-Albrecht,[§] Wolfgang Knoll,[∥] Martin Steinhart,[⊥,#,*] Bahram Djafari-Rouhani,[‡] and George Fytas[†,▽,*]

[†]Max Planck Institute for Polymer Research, Ackermannweg 10, 55128 Mainz, Germany, [‡]Institut d'Electronique de Microélectronique et de Nanotechnologie, UMR CNRS 8520, Université de Lille1 Sciences et Technologies, 59652 Villeneuve d'Ascq, France, [§]Institute of Physics, Martin Luther University Halle-Wittenberg, Germany, [⊥]Max Planck Institute of Microstructure Physics, Weinberg 2, D-06120 Halle, Germany, [∥]Austrian Institute of Technology GmbH, Tech Gate Vienna, Donau-City-Street 1, 1220 Vienna, Austria, [#]Institute for Chemistry, University of Osnabrück, Barabarastrasse, 7, D-46069 Osnabrück, and [▽]Department of Materials Science and Technology and FORTH, 71110 Heraklion, Greece. [◆]Current address: Laboratoire d'Optique Biomédicale, Ecole Polytechnique Fédérale de Lausanne, EPFL STI IMT LOB, BM 5.139, Station 17, CH-1015 Lausanne, Switzerland.

ABSTRACT Anodic aluminum oxide (AAO) containing arrays of aligned cylindrical nanopores infiltrated with polymers is a well-defined model system for the study of hypersound propagation in polymer nanocomposites. Hypersonic phononic properties of AAO/polymer nanocomposites such as phonon localization and anisotropic sound propagation can be tailored by adjusting elastic contrast and density contrast between the components. Changes in density and elastic properties of the component located in the nanopores induced by phase transitions allow reversible modification of the phononic band structure and mode switching. As example in case, the crystallization and melting of poly(vinylidene difluoride) inside AAO was investigated.

KEYWORDS: nanocomposites · mechanical properties · phononic dispersion relations · Brillouin light scattering

Nanocomposites are a class of materials, the importance of which for a broad variety of industrial applications cannot be overestimated. Commonly, they are characterized by irregular structure, and clustering of dispersed filler particles may significantly deteriorate their properties. Up to now, their physics is not satisfactorily understood, and their design on the mesoscopic or even molecular scale is still challenging. However, it would be an intriguing perspective to design nanocomposites that exhibit specific functions related to tailored structural anisotropy or to likewise tailored, well-defined periodicity. Ultimately, such advanced nanocomposites would show smart behavior or stimuli-responsive properties. Whereas tailoring of the mechanical properties and the electric conductivity of nanocomposites has received much attention, the lack of control over their morphology has prevented the systematic tuning of their phononic properties.

Sound can propagate through solids as longitudinal wave with a longitudinal sound velocity c_l or as a transverse wave having a transverse sound velocity c_t. In general, media through which sound waves propagate can be classified according to their elastic impedance $Z = \rho c$, where ρ denotes the mass density of the medium and c is the sound velocity in the medium. In periodic composite media consisting of components having different elastic impedances, the periodic structure strongly influences sound propagation on condition that sound wavelength and periodicity of the medium are commensurate. The phononic band structure of periodic composite media depends on differences in mass densities, sound velocities and elastic impedances between the components, the volume fractions of the components, and the symmetry and morphology of the lattice they constitute.

Up to now, predominantly phononic composite systems with characteristic feature sizes on the micrometer scale and above have been employed to manipulate the propagation of sound[1−6] and to generate phononic band gaps prohibiting sound propagation for specific wavelengths.[7−10] Hence, efforts to engineer the band gap frequency region and the flow of elastic energy outside the band gap have been focused on the sonic and ultrasonic frequency range,[2−4,11] and research has predominantly aimed at the search of absolute band gaps in solid structures with lattice constants in the millimeter range.[10,12] Whereas only few attempts to adapt concepts for functional phononic bandgap structures to the GHz frequency range have been

*Address correspondence to martin.steinhart@uos.de, fytas@mpip-mainz.mpg.de.

Received for review March 12, 2010 and accepted May 19, 2010.

Published online May 28, 2010. 10.1021/nn100519h

TABLE 1. Bulk Sound Velocities and Bulk Densities of the Materials Used, as Well as the Elastic Impedance Contrasts of the Corresponding Nanocomposites

material	c_l (m/s)	c_t (m/s)	ρ (kg/m^3)	ΔZ
AAO	7300[a]	3750[a]	2880 ± 355[d]	
PDMS	1050 ± 20[b]		974[e]	19.6
PEG	1900[b]		1040[f]	9.64
PVDF melt	1220[c]		1490[g]	10.6
α-PVDF	2480[b]	775[i]	1900[h]	3.46

[a]Reference 25. [b]Measured by BLS at room temperature (20 °C). [c]Measured by BLS at 180 °C. [d]Determined by gravimetry. [e]Density of PDMS with a viscosity-average molecular weight of 105 g/mol was determined using two pycnometers at 20 °C.[28] [f]Density of hydroxyl-terminated PEG with a molecular weight of 300 g/mol was determined at 30 °C.[29] [g]Density of PVDF with a molecular weight of 197 000 g/mol was determined at 180 °C.[30] [h]Density was determined for α-phase of PVDF at room temperature.[31] [i]The transverse sound velocity was determined by ultrasonic measurement at room temperature.[32]

reported,[13−16] despite the potential of such systems for a plethora of applications,[17] predictive understanding of the properties of hypersonic systems and of principles for their rational engineering is still premature. Nanocomposites characterized by periodic elastic impedance contrast variations on nanoscopic length scales could be the starting point for the design of highly efficient heat management and phonon management systems operated in the hypersonic frequency range.

Self-ordered nanoporous anodic aluminum oxide (AAO) obtained by mild anodization[18−20] contains arrays of aligned nanopores having narrow pore diameter distributions. The nanopores, which are uniform in diameter along their entire depth, are arranged in hexagonal arrays characterized by grains extending 10−20 lattice constants. Whereas the fabrication of one-dimensional nanostructures using disordered and self-ordered AAO as a shape-defining mold is well established,[21−23] only little effort has been made to explore self-ordered AAO as a rigid, inorganic scaffold in model nanocomposites.[23−26] This is astounding since organic/inorganic hybrid systems based on self-ordered AAO combine, in contrast to disordered filler/matrix systems, well-defined morphology and likewise well-defined anisotropy. Using the longitudinal sound velocity of AAO, $c_{l,AAO}$, as well as the bulk density ρ_f and the bulk longitudinal sound velocity c_f of a fluid infiltrated into AAO, the contrast ΔZ in the elastic impedances of AAO and an infiltrated fluid can be calculated as follows:

$$\Delta Z = \frac{\rho_{AAO} c_{l,AAO}}{\rho_f c_f} - 1 \qquad (1)$$

The mass density of AAO $\rho_{AAO} = 2880 \pm 355$ kg/m^3, as gravimetrically determined, is typically two to three times larger than that of infiltrated soft materials (*cf.* Table 1). Moreover, the exceptionally high longitudinal ($c_{l,AAO} = 7300$ m/s) and transverse ($c_{t,AAO} = 3750$ m/s) sound velocities of AAO[25] significantly exceed those of air ($c_l = 340$ m/s) or soft materials deposited into the nanopores (*cf.* Table 1). Hence, nanocomposites consisting of AAO and an infiltrated fluid typically have pronounced elastic impedance contrasts. As a result, even localization of hypersonic modes can occur.[25] AAO-based membrane configurations are ideal model systems for the investigation of hypersound propagation, because their periodicity in elastic impedance contrast imposed by the morphology of the AAO matches the length scales required to manipulate hypersound in the GHz frequency range. Sound waves propagating perpendicular to the long axes of the nanopores in the AAO scaffold (in-plane) experience elastic impedance contrast, whereas sound waves propagating along a direction parallel to the nanopore axes (out-of-plane) experience predominantly a homogeneous medium. Therefore, AAO-based nanocomposites should also be promising model systems to realize directed sound propagation along the nanopores.

Since AAO is transparent to UV light and visible light, Brillouin light scattering spectroscopy (BLS),[13,27] a nondestructive optical technique to probe the phonon dispersion relation that utilizes scattering of the incident laser light by random thermal phonons, can be applied. The scattering vector $\mathbf{q} = \mathbf{k}_s - \mathbf{k}_i$ is defined by the wavevectors of the scattered ($\mathbf{k}_s$) and incident ($\mathbf{k}_i$) photons, as illustrated in Scheme 1. Scattering vectors $\mathbf{q}_\perp$ representing in-plane phonon propagation are oriented perpendicular to the pore axes. Their magnitudes $q_\perp = (4\pi/\lambda) \sin(\theta/2)$ depend on the scattering angle θ and the wavelength of the incident laser light, but are independent of the refractive index of the medium. The scattering vectors $\mathbf{q}_\parallel$ representing out-of-plane phonon propagation are oriented parallel to the pore axes. Their magnitudes $q_\parallel = (4\pi n/\lambda) \sin(\theta/2)$ depend on the effective refractive index of the medium.

Here we present an in-depth study of the phononic properties of AAO-based impedance-contrast nanocomposites. In all experiments reported below, we used self-ordered AAO with a lattice constant $a \approx 100$ nm and a pore diameter $d \approx 60$ nm (Figure 1), which was prepared according to Masuda's two-step anodization process,[18] followed by isotropic etching with oxalic acid to widen the nanopores. Liquid poly(dimethyl siloxane) (PDMS), liquid polyethylene glycol (PEG), liquid poly(vinylidene difluoride) (PVDF), and semicrystalline PVDF were selected as soft model components (Table 1). PDMS has a low mass density and a low bulk sound velocity so that AAO/PDMS nanocomposites exhibit a high ΔZ value of 19.6 (Table 1). Liquid PEG has a significantly higher longitudinal bulk sound velocity than liquid PDMS, whereas both liquids have similar densities so that AAO/PEG nanocomposites have a lower elastic impedance contrast than AAO/PDMS nanocomposites. PVDF melts have a significantly higher bulk density than PDMS, whereas the bulk longitudinal sound velocities are comparable so that the elastic impedance contrast in AAO/PDMS nanocomposites is again higher than in

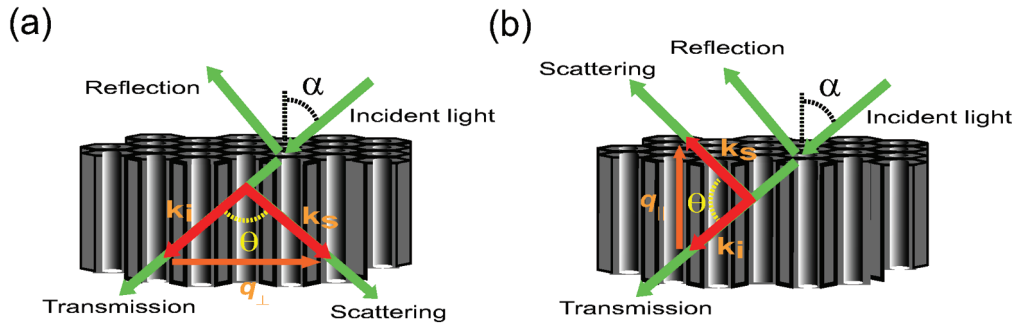

Scheme 1. BLS spectroscopy setup. The phonon wave vector q for a scattering angle θ (twice the incidence angle α) can be oriented either perpendicular or parallel to the long axes of the nanopores in the AAO scaffold. Perpendicular orientation of phonon wavevector $\mathbf{q}_\perp$ corresponds to transmission geometry (panel a), and parallel orientation of phonon wavevector $\mathbf{q}_\parallel$ corresponds to reflection geometry (panel b). BLS spectra for different wavevectors $\mathbf{q}_\perp$ or $\mathbf{q}_\parallel$ are accessible by appropriate positioning of the AAO membrane (adjustment of incident angle α) and the detector (adjustment of scattering angle θ). In-plane hypersound propagation perpendicular to the long axes of the AAO nanopores can be probed by measurements in transmission geometry (panel a); out-of-plane hypersound propagation parallel to the long axes or the AAO nanpores can be probed by measurements in reflection geometry (panel b).

AAO/molten PVDF nanocomposites; molten PVDF has a higher bulk density, a comparable elastic impedance contrast, and a lower bulk sound velocity than PEG. Therefore, these three model soft components allow systematically elucidating the influence of the bulk sound velocity and the bulk density of the infiltrated material in AAO nanocomposites on their hypersonic properties.

Up to now, elastic impedance contrast nanocomposites have been considered as static phononic systems. Using PVDF as a semicrystalline model polymer, we finally demonstrate that the exploitation of first order phase transitions such as melting and crystallization allows modifying the elastic properties and densities of materials residing in the nanopores. In turn, the phononic band structure, the density of states and ultimately the hypersonic acoustic properties of AAO-based impedance-contrast nanocomposites can be switched.

RESULTS AND DISCUSSION

AAO/PDMS: A Model System with High Elastic Contrast. Studies of nanocomposites consisting of PDMS matrices filled with silica nanoparticles based on NMR spectroscopy,[33,34] dielectric relaxation spectroscopy,[35] and dynamic mechanical analyses[36] revealed that the filler particles are surrounded by several PDMS layers characterized by restricted segmental mobility. In these rigid amorphous layers, glass transitions at higher temperatures or lower frequencies than in the bulk occurred. Direct evidence for modified dynamics in the GHz and THz range characterized by reduced segmental mobility was obtained by quasielastic neutron scattering.[37] The overall thickness of the PDMS interphase, as determined by various methods for a broad range of molecular weights, was reported to range from 1 to 5 nm.[33,36−38] Molten PDMS with a molecular weight of ~3700 g/mol (~50 repeat units) located between two molecularly smooth mica surfaces formed layered structures near the solid interfaces.[39] In films with thicknesses below <5 nm, entropic repulsion attributed to conformational restrictions of the PDMS molecules was an oscillatory function of film thickness with a repeat spacing corresponding to the width of the polymer molecule. The oscillatory force ranged 7−8 chain widths (about 5 nm), whereas dynamic force measurements revealed a hydrodynamic thickness of the immobilized layer of 2−3 nm.[39] Evmenenko *et al.* evidenced molecular layering for films thinner than 9 nm consisting of low molecular weight PDMS (M < 1000 g/mol) deposited onto a smooth Si wafer by X-ray reflectivity.[40] In thick films of PDMS with molecular weights of 3780 g/mol and above, no layered structure was found to be stable for entropic reasons, but interphases with a thickness of a few nm appeared.[38] Moreover, NMR investigations revealed that thin films of PDMS with molecular weights of the order of 10 000 g/mol deposited from diluted solutions onto the pore walls of AAO are arranged in discrete layers characterized by stepwise increase in motional freedom.[41,42]

In the works discussed above, predominantly disordered PDMS nanocomposite systems that do not allow systematically probing phononic properties were considered. We have previously studied AAO with a lattice constant a of 100 nm, a pore depth of 20 μm, and pore diameters d ranging from 35 to 85 nm infiltrated with

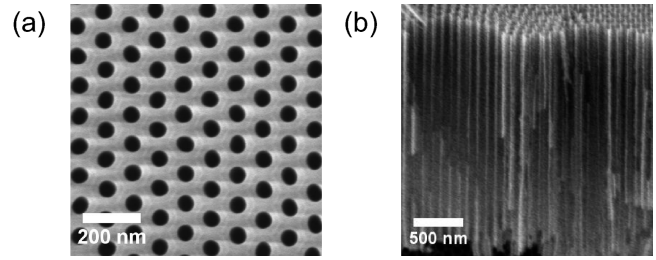

Figure 1. Scanning electron microscopy (SEM) images of self-ordered AAO obtained with oxalic acid as electrolyte solution: (a) top view and (b) cross sectional image.

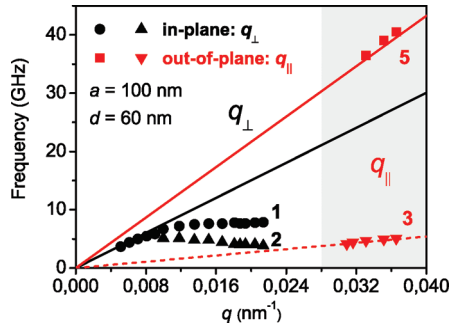

Figure 2. Experimental dispersion diagram showing in-plane ($\mathbf{q}_\perp$) and out-of-plane ($\mathbf{q}_\parallel$) longitudinal phononic branches 1−3 and 5 in PDMS-filled AAO scaffolds (d = 60 nm; a = 100 nm). The black and red solid lines represent the effective sound velocities along the in-plane directions perpendicular to the pore axes (data points in the unshaded area) and along the out-of-plane direction parallel to the pore axes (data points in the light gray area). The bending of acoustic effective medium branch 1 at high $q_\perp$ values is related to interaction with a flat band confined to the fluid PDMS inside the nanopores and, therefore, indicative of mode localization. Branch 2 is probably related to the presence of a rigid PDMS interphase in the vicinity of the pore walls. The large mechanical anisotropy of the PDMS/AAO nanocomposites is apparent from the different slopes of the red (5) and black (1) lines. Branch 3 represents a phonon predominantly localized in the PDMS inside the nanopores and is, therefore, indicative of directed sound propagation.

trimethylsilane-terminated oligomeric PDMS with a molecular weight of 1350 g/mol.[25] Figure 2 shows exemplary dispersion relations $\omega(\mathbf{q})$ in PDMS-filled AAO with $d = 60$ nm, $a = 100$ nm and a porosity $p = \pi d^2/(2\sqrt{3}a^2) = 32\%$ for in-plane phonon propagation perpendicular to the pore axes (denoted by wavevector $\mathbf{q}_\perp$) and for out-of-plane phonon propagation parallel to the pore axes (denoted by wavevector $\mathbf{q}_\parallel$). The characteristic features of the dispersion relations $\omega(\mathbf{q})$ displayed in Figure 2 can be summarized as follows.

(i) The acoustic ($\omega \approx \mathbf{q}$) out-of-plane phonon represented by branch **5** and the acoustic in-plane phonon represented by branch **1** recognize PDMS-filled AAO as effective medium at low wave vectors and hence long wavelengths. However, the AAO/PDMS nanocomposites exhibit different effective medium sound velocities parallel (branch **5**) and perpendicular (branch **1**) to the nanopores. According to simulations, the out-of-plane branch (**5**) propagates mainly through the AAO scaffold with a sound velocity of 6930 m/s, whereas its counterpart, the in-plane branch (**1**), propagates through both the AAO scaffold and the polymer located in the nanopores with a slower sound velocity of 4520 m/s. Hence, the longitudinal moduli (ρc_l^2) along the two directions correspond to an anisotropy ratio of 2.3.

(ii) The group velocity belonging to acoustic in-plane branch **1** at high **q** values becomes almost zero. As revealed by simulations, the bending is caused by the interaction of branch **1** with a flat band $f_l \approx 8.5$ GHz corresponding to a confined mode inside the PDMS cylinders. The frequency f_l depends on the pore diameter and the nature of the material in the nanopores.

(iii) Out-of-plane phonon guiding represented by branch **3** is realized when the nanopores are filled with PDMS, thus opening a new channel for the directed flow of the elastic energy. As obvious from simulations, the acoustic branch **3** propagates through nanopores containing PDMS with a sound velocity of 980 m/s, which is slower than the sound velocity in bulk PDMS ($c_{lPDMS} = 1050 \pm 20$ m/s). This channel of phonon propagation becomes inactive in AAO with air pores.

(iv) A flat in-plane branch **2**, which does not occur in simulations assuming a homogeneous liquid PDMS phase inside the AAO nanopores, might be related to a solid-like PDMS interphase on the pore walls. Consistent with these findings, the experimentally observed flat branch **2** with frequency f_i seen in Figure 2 could be reproduced in simulations of the hypersonic dispersion in AAO/PDMS nanocomposites by using models involving a solid-like PDMS interphase on the pore walls. Branch **2** is, first and foremost, sensitive to the transverse sound velocity c_t and to the assumed thickness of the PDMS interphase at the pore walls; f_i increases either by increasing c_t or by decreasing the thickness. The displacement of the elastic field is essentially confined to the PDMS interphase on the walls of the nanopores and polarized parallel to the nanopore axes.

AAO/PEG: A Model System with Low Elastic Contrast. Like PDMS, low-molecular-weight PEG is an isotropic liquid at room temperature. However, the longitudinal sound velocity of PEG is significantly higher than that of PDMS. Therefore, AAO/PEG nanocomposites have a significantly smaller elastic impedance contrast ΔZ than AAO/PDMS nanocomposites; ΔZ drops from 19.6 in the system AAO/PDMS to 9.64 in the system AAO/PEG (Table 1). The comparison of PEG-filled AAO and PDMS-filled AAO allows an elucidation of whether high elastic contrast is required to realize mode localization as well as directional flow of elastic energy, and whether high elastic contrast is a prerequisite for the occurrence of interphase-sensitive branches. It is reasonable to assume that lower elastic contrast between AAO and a soft component residing in its nanopores affects the extent of phonon localization, which is represented by the bending of the acoustic branch **1** in Figure 2.

To verify these predictions, we studied the in-plane ($\mathbf{q}_\perp$) sound propagation in AAO ($d \approx 60$ nm and $a \approx 100$ nm) filled with hydroxyl-terminated liquid PEG. Three modes are resolved in the exemplary BLS spectrum, as indicated by the Lorentzian contributions (Figure 3a). The peak denoted "PEG" with a frequency $f_{PEG} \approx 5$ GHz (at $q_\perp = 0.0167$ nm^{-1}) is attributed to a bulk PEG layer on top of the AAO surface used as an internal reference, since at f_{PEG} homogeneous acoustic behavior with a sound velocity $c_{l,PEG}$ ($= 2\pi f_{PEG}/q_\perp$) $= 1850 \pm 30$ m/s is apparent. Within experimental error, this value corresponds to the longitudinal sound velocity of bulk PEG. For comparison, a BLS spectrum of a PDMS/AAO nanocomposite using AAO with the same specifi-

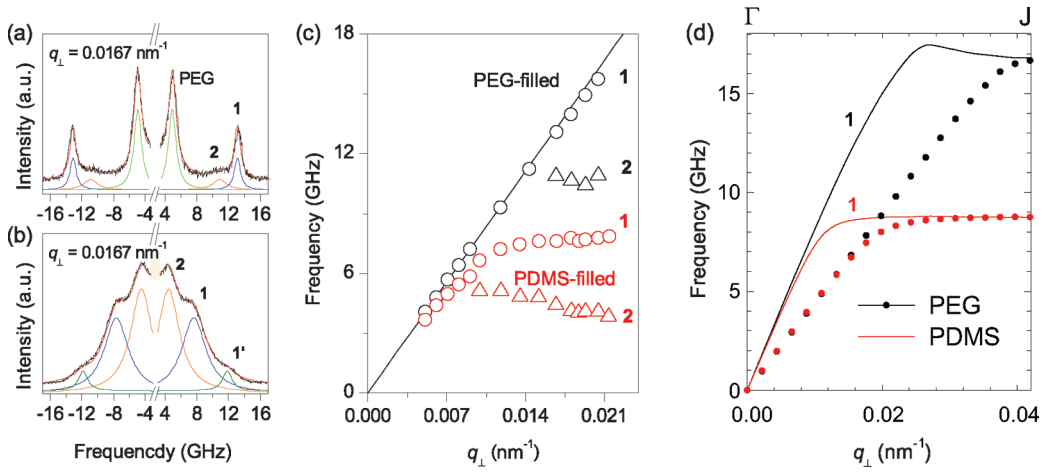

Figure 3. Comparison of the systems AAO/PEG and AAO/PDMS using AAO with d = 60 nm and a = 100 nm. (a,b) BLS spectra at $q_\perp$ = 0.0167 nm^{-1} representing in-plane phonon propagation (a) in PEG-filled AAO and (b) in PDMS-filled AAO. The red solid lines are the sums of up to three Lorentzian lines. (c) Experimental in-plane dispersion relations of the longitudinal acoustic branch 1 (black open circles) and the weak flat branch 2 (black open triangles) in PEG-filled AAO. The slope of branch 1 fitted by the black solid line is representative of the effective velocity of in-plane sound propagation in AAO/PEG nanocomposites. Experimental dispersion relations of in-plane branches 1 (red open circles) and 2 (red open triangles) of the system AAO/PDMS are shown for comparison. (d) Simulated phononic dispersion relations of longitudinal mode 1 for PEG-filled AAO (black solid line) and PDMS-filled AAO (red solid line). The black and red dots represent transverse modes for PEG-filled AAO and PDMS-filled AAO, respectively.

cations ($d \approx 60$ nm and $a \approx 100$ nm) and recorded at the same $\mathbf{q}_\perp$ (0.0167 nm^{-1}) is shown in Figure 3b, which contains peaks belonging to the acoustic branch **1** and the interphase-sensitive branch **2**.

The experimental dispersion diagrams for in-plane phonon propagation in PEG-filled AAO and, for comparison, in PDMS-filled AAO are depicted in Figure 3c. The linear dispersion of the acoustic in-plane branch **1** indicated by the straight solid line in Figure 3c represents longitudinal phonon propagation at long wavelengths probing a homogeneous medium, and its slope is representative of the corresponding longitudinal sound velocity. Consistent with the fact that PEG has a higher longitudinal sound velocity than PDMS (Table 1), the effective longitudinal sound velocity in the AAO/PEG nanocomposites (c_l = 5040 m/s) is higher than that in AAO/PDMS nanocomposites (c_l = 4520 m/s). The clear bending of the acoustic branch **1** at $f_l \approx 8.5$ GHz, which is related to the interaction with a flat band, is a characteristic feature of the dispersion in AAO/PDMS nanocomposites and indicates the presence of a mode confined to the PDMS cylinders (Figure 3c). However, in the corresponding frequency range, acoustic branch **1** in the dispersion diagrams of the system AAO/PEG shows only subtle deviation from linear dispersion behavior starting at a frequency of about 15 GHz; bending of branch **1** is not observed within the experimentally covered $q_\perp$ range (Figure 3c).

Computations of the in-plane dispersion curves of AAO/PEG and AAO/PDMS nanocomposites along the symmetry direction ΓJ (assuming that the AAO exhibits a "single crystalline" degree of order) suggest that the substitution of PDMS by PEG shifts the bending of branch **1** to a higher $\mathbf{q}_\perp$ value of 0.024 nm^{-1} and to a higher frequency $f_l \approx 17.5$ GHz (Figure 3d). This outcome can be interpreted as the signature of significantly less pronounced phonon localization in AAO/PEG nanocomposites as compared to AAO/PDMS nanocomposites. Since the densities of PDMS and PEG are similar, the halving of ΔZ (Table 1) related to the higher longitudinal sound velocity in PEG remains as a possible origin of this difference.

A second characteristic feature seen in the dispersion diagrams of AAO/PDMS nanocomposites is a strong, interphase-sensitive flat in-plane branch **2** (Figure 3b) in the frequency range from about 3.5 to 5 GHz (Figure 3c). Its counterpart in the dispersion diagrams of the system AAO/PEG, however, is a very weak flat branch **2** (Figure 3a) appearing at higher frequencies around 10.5 GHz (Figure 3c). In the BLS spectra of the AAO/PEG nanocomposites, the intensity ratios of peak **2** belonging to branch **2** and peak **1** belonging to branch **1**, $I_{2_{PEG}}/I_{1_{PEG}}$, amounts to ~0.45 and is by a factor of ~3 smaller than $I_{2_{PDMS}}/I_{1_{PDMS}}$ in the BLS spectra of AAO/PDMS nanocomposites (*cf.* Figure 3a,b). This outcome corroborates the notion that flat branch **2** is related to the presence of an interphase of the infiltrated liquid at the pore walls, which is characterized by more solidlike properties than in the center of the pores. It is difficult to precisely capture the frequency of branch **2** in theoretical computations since values for both c_t and the thickness of the interphase layer have to be assumed. Nevertheless, it is reasonable to assume the presence of a PEG interphase because the hydroxyl end groups of the PEG, and possibly the oxygen atoms in the PEG backbone, form hydrogen bonds with the pore walls. However, as compared to the system AAO/PDMS, the relatively small elastic impedance contrast and the high

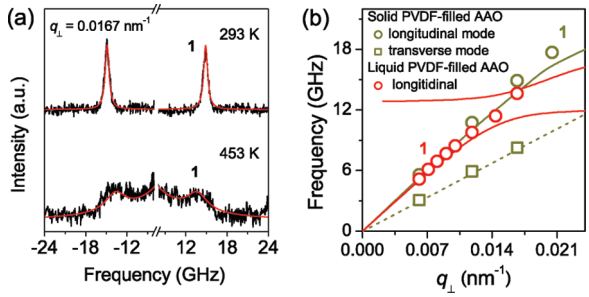

Figure 4. (a) In-plane BLS spectra of PVDF-filled AAO (d = 60 nm; a = 100 nm) measured at 293 K (PVDF is semicrystalline) and at 453 K (PVDF is liquid) for $q_\perp$ = 0.0167 nm^{-1}. (b) Experimental and simulated dispersion relations of in-plane ($\mathbf{q}_\perp$) acoustic modes in AAO containing semicrystalline PVDF at 293 K and AAO containing liquid PVDF at 453 K as indicated in panel a. The solid and dashed dark yellow lines are simulated dispersion relations for the longitudinal mode and the transverse mode at 293 K, respectively. The dark yellow open circles and squares are the corresponding experimental dispersion relations. The solid red lines are simulated dispersion relations for the longitudinal mode at 453 K. The red open circles are the corresponding experimental dispersion relations.

longitudinal sound velocity in PEG result in less pronounced interphase-related features in the phononic dispersion diagrams of the system AAO/PEG.

Switching Phononic Properties of the System AAO/PVDF by Crystallization and Melting of PVDF. External stimuli, for example temperature changes, may induce transitions such as crystallization, gelation, magnetization, or the formation of mesophases in the soft component residing in nanopores of the AAO scaffold. Correspondingly, phononic properties and phononic band structures of the nanocomposites, as well as their acousto-optical interactions, are modified. From a fundamental point of view, solidification or softening of infiltrated materials may allow further elucidation of the origin of observed phononic branches in the band diagrams. For a simple proof of concept, we investigated the modification of the dispersion for both in-plane and out-of-plane sound propagation associated with crystallization and melting of PVDF infiltrated into AAO. PVDF is representative of the important class of vinylidene-based fluoropolymers, which may exhibit, depending on the crystal modification, ferroelectric properties.[43] PVDF was selected as a model component because its crystallization inside the nanopores of AAO, which yields the monoclinic α polymorph,[44] was intensively studied by wide-angle X-ray scattering and differential scanning calorimetry.[45,46] Martin *et al.* studied the dynamics of the amorphous regions in semicrystalline PVDF confined to AAO.[47] Moreover, semicrystalline α-PVDF has a significantly higher bulk density and likewise a significantly higher bulk sound velocity than molten PVDF (Table 1) so that the transition between both states should be accompanied by pronounced changes in the phononic band structure. The PVDF in the nanopores of the AAO melted at ~437 K (Supporting Information, Figure S1). Therefore, BLS spectra of the system AAO/solid PVDF could be obtained at 293 K and BLS spectra of the system AAO/liquid PVDF at 453 K.

BLS spectra measured at $q_\perp$ = 0.0167 nm^{-1} representative of in-plane sound propagation are shown in Figure 4a. For AAO containing semicrystalline PVDF, the BLS spectrum displays only a single doublet associated with a longitudinal phonon **1**. However, although the BLS spectrum of AAO containing liquid PVDF also displays a single doublet at almost the same frequency, the peaks became broader and slightly shifted to lower frequencies. The occurrence of broad peaks supports the notion that at high temperatures relaxation processes in liquid PVDF lead to phonon damping. The experimental dispersion relations superposed on the theoretical dispersion relations of both semicrystalline and liquid PVDF-filled AAO are shown in Figure 4b. Only simulated branches captured experimentally are displayed, while the complete set of simulated dispersion curves is shown in Figure S2. In the case of the system AAO/liquid PVDF, only the longitudinal acoustic in-plane branch **1** was experimentally captured (red open circles, experimental values; red solid lines, computed curves). Similar to the behavior of in-plane branch **1** in the systems AAO/PDMS and AAO/PEG, its interaction of with a flat band attributed to a mode localized in the liquid-PVDF cylinders leads the bending of the acoustic part of branch **1**. As a result, a narrow band gap opens at frequencies near 12 GHz.

In the case of the system AAO/solid PVDF, BLS measurements were consistent with simulations and revealed the occurrence of an acoustic transverse branch (experimental values, dark yellow open squares; computed curve, dark yellow dashed line) and an acoustic longitudinal branch (experimental values, dark yellow open circles; computed curve, dark yellow solid line). The longitudinal phonon **1** shows linear dispersion but no bending up to $q_\perp \sim 0.02$ nm^{-1}. At a temperature of 453 K, the in-plane acoustic branch **1** propagates through both the AAO scaffold and the liquid PVDF located in the nanopores with an effective medium sound velocity c_l = 5370 m/s, which increases only by about 4% in the system AAO/solid PVDF at a temperature of 293 K (Table 2).

The BLS spectra representing the out-of-plane phonon propagation measured at $q_\parallel$ = 0.0368 nm^{-1} change drastically upon the melting of PVDF (Figure 5a,b). Mode **4** occurring at a frequency of ~20 GHz in the spectrum of the system AAO/solid PVDF disappears. Instead, a weak and broad peak at about 6 GHz, the width of which indicates that an almost overdamped branch **3** propagates through the nanopores containing liquid PVDF, is observed in the spectrum of AAO/liquid PVDF. However, the longitudinal effective medium mode **5** occurring in the spectra of the system AAO/solid PVDF is conserved in the system AAO/liquid PVDF. The experimental dispersion curves representing out-of-plane hypersound propagation, which are super-

TABLE 2. Experimental and Computed Sound Velocities in AAO/Polymer Nanocomposites and Bending Frequencies of Mode 1

system	c_1 (m/s)[a]	$f_{i,1}$[d] (GHz)	c_5 (m/s)[a]	c_3 (m/s)[a]
PDMS/AAO	4520/4740 (−4%)	~8.5[e]	6910/6780 (2%)	870/950 (−8%)
PEG/AAO	5040/5125 (−2%)	~17.5[f]	6550/6690 (−2%)	1830/1890 (−3%)
$PVDF_{(l)}$/AAO[b]	5370/5200 (−3%)	~12[f]	6810/7060 (−4%)	1060/1270 (−18%)
$PVDF_{(s)}$/AAO[c]	5550/5400 (3%)		7170/6950 (3%)	

[a]Experimental/simulation (deviation %). [b]Measured at 453 K. [c]Measured at 293 K. [d]Frequency at which bending of acoustic in-plane mode **1** occurs. [e]According to the experimental dispersion relation at 293 °C. [f]According to simulations.

posed onto the simulated dispersion relations, are displayed in Figure 5c. The sound velocity of mode **5** does not change significantly when PVDF residing in the nanopores transforms from semicrystalline (7170 m/s) to liquid (6810 m/s). Mode **4** of the system AAO/solid PVDF and mode **3** of the system AAO/liquid PVDF have very different theoretical dispersion relations. As in the system AAO/PDMS, mode **3** is mainly confined to the fluid inside the nanopores and has a longitudinal character. However, mode **4** experimentally detected in AAO/solid PVDF is apparently related to the transverse branch appearing in the computed dispersion diagram. Within the experimentally covered $\mathbf{q}_\parallel$ range, mode **4** interacts smoothly with an almost flat branch at 16 GHz. The mechanical anisotropies of the systems AAO/liquid PVDF and AAO/solid PVDF, represented by the ratio of the squares of the sound velocities c_5 and c_1 of effective medium out-of-plane mode **5** and effective medium in-plane mode **1**, c_5^2/c_1^2, are quite similar and amount to about 1.6. This value is significantly smaller than that (2.3) of the system AAO/PDMS (Table 2).

The amplitudes of the three components U_x, U_y, and U_z of the acoustic field belonging to point *A* on mode **4** ($q_\parallel = 0.0368$ nm^{-1}; $f = 19.4$ GHz; as indicated in Figure 5c), are sketched in Figure 6. The longitudinal component U_z is oriented parallel, and the transverse components U_x and U_y are oriented perpendicular to the long axes of the semicrystalline PVDF cylinders located in the nanopores of the AAO scaffold, with component U_x being parallel to the ΓJ direction of the Brillouin zone. The transverse components U_x and U_y of the displacement field are spread over the whole unit cell (Figure 6a), although their magnitude is higher in the semicrystalline PVDF cylinders. However, the longitudinal component U_z is clearly confined inside the semicrystalline cylinders and practically vanishes in the AAO scaffold.

Three major effects in the hypersonic band diagrams of AAO/PVDF nanocomposites are associated with the crystallization of PVDF inside the nanopores of AAO. (i) The BLS peaks belonging to in-plane acoustic mode **1** become significantly narrower due to the lower elastic energy dissipation, and the corresponding sound velocity derived from the in-plane dispersion diagram becomes marginally faster. (ii) Out-of-plane dispersion is characterized by the appearance of a new nonacoustic mode **4** at ~20 GHz in place of acoustic mode **3** at ~6 GHz. (iii) The sound velocity of the longitudinal effective medium mode **5** does not change significantly when the PVDF residing in the nanopores transforms from liquid to semicrystalline.

Comparison of the Systems AAO/Liquid PVDF, AAO/PEG, and AAO/PDMS. The comparison of the systems AAO/liquid PVDF, AAO/PEG, and AAO/PDMS allows elucidating the dependence of the phononic properties of the AAO/polymer nanocomposites on the nature of the polymeric components. AAO/liquid PVDF and AAO/PEG possess similar ΔZ values, which amount to about half the ΔZ value of the system AAO/PDMS. However, in contrast to PEG, which is characterized by high longitudinal sound velocity and relatively low density, PVDF melts combine high bulk density and relatively low longitudinal sound velocity (Table 1). Therefore, the system AAO/liquid PVDF complements the comparison of the systems AAO/PDMS and AAO/PEG. Table 2 summarizes the experimental and computed values of the sound phase velocities in the AAO/polymer nanocomposites and the frequency f_i of the flat band interacting with mode **1**.

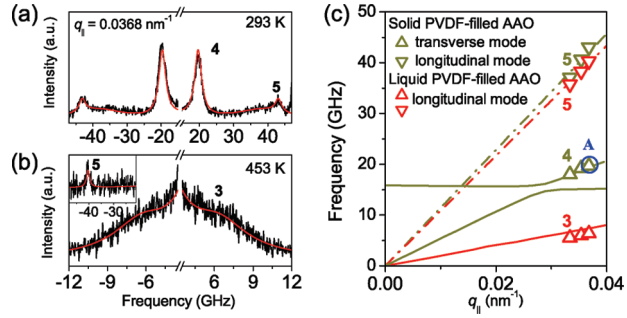

Figure 5. Out-of-plane BLS spectra of PVDF-filled AAO ($d = 60$ nm; $a = 100$ nm) measured (a) at 293 K (PVDF is semicrystalline) and (b) at 453 K (PVDF is liquid) for $q_\parallel = 0.0368$ nm^{-1}. The inset in panel b shows the peak belonging to mode 5 at about 40 GHz. (c) Dispersion relations of the out-of-plane ($\mathbf{q}_\parallel$) acoustic modes in the systems AAO/solid PVDF at 293 K and AAO/liquid PVDF at 453 K, as indicated in panels a and b. The solid and dashed dark yellow lines are simulated dispersion relations for transverse mode 4 and longitudinal mode 5 at 293 K, respectively. The dark yellow open triangles pointing upward represent experimental transverse mode 4 and the dark yellow open triangles pointing downward experimental longitudinal mode 5 at 293 K. The solid and dashed red lines are simulated dispersion relations for the longitudinal modes 3 and 5 at 453 K. The red open triangles pointing upward represent experimental longitudinal mode 3 and the red open triangles pointing downward experimental longitudinal mode 5 at 453 K.

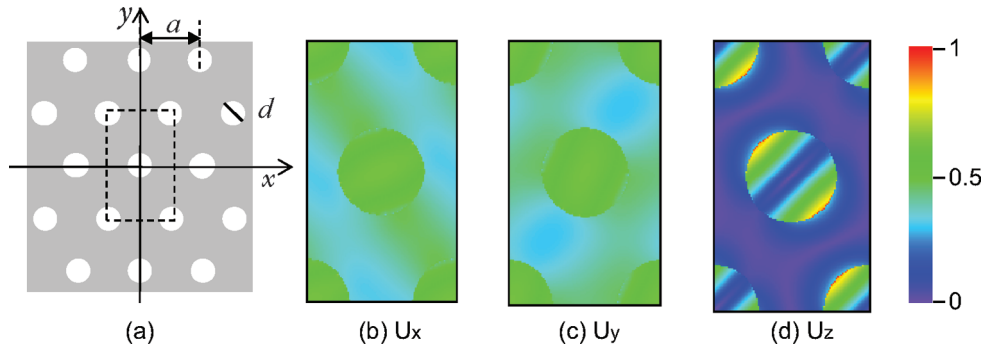

Figure 6. Map of the amplitude of the acoustic field at point *A* indicated in Figure 5c on transverse out-of-plane branch 4 of the system AAO/solid PVDF: (a) schematic representation of the unit cell inside the hexagonal array; (b) transversal component U_x, which is oriented along the ΓJ direction of the Brillouin zone and perpendicular to the long axes of the nanopores in the AAO; (c) transversal component U_y, which is oriented perpendicular to the long axes of the nanopores in the AAO; and (d) longitudinal component U_z, which is oriented parallel to the long axes of the nanopores in the AAO scaffold.

Acoustic effective medium mode **1** is related to in-plane phonon propagation. Its bending at high $q_\perp$ (Table 2) is a peculiar feature appearing in the experimental dispersion diagrams of the system AAO/PDMS (Figure 2). At the bending frequency f_l, a flat mode confined to the PDMS inside the nanopores of the AAO interacts with mode **1**, the bending of which, therefore, indicates mode localization in the PDMS cylinders. In contrast to the system AAO/PDMS, bending of mode **1** does not appear in the experimental dispersion diagrams of the systems AAO/PEG (Figure 3c) and AAO/liquid PVDF (Figure 4b). However, simulations revealed that the flat band confined to the fluid cylinders causing the bending of mode **1** in AAO/PEG is shifted to high frequencies not covered experimentally. The flat band responsible for the predicted bending of branch **1** in the system AAO/liquid PVDF appears at $f_l \approx 12$ GHz in the computed in-plane band diagram seen in Figure 4b. The absence of a signature of the bending in the experimental dispersion relation (for $q_\perp > 0.017$ nm^{-1}) is probably related to the large width of the peaks belonging to branch **1** in the BLS spectra (Figure 4a). Apparently, higher longitudinal sound velocities and correspondingly smaller elastic impedance contrasts of the fluid infiltrated into the AAO (Table 1) shift the bending of acoustic in-plane mode **1** to higher frequencies and reduce the extent of phonon localization inside the fluid cylinders.

Directed phonon propagation along the nanopores through the infiltrated fluid is represented by the much softer (lower sound velocity) acoustic out-of-plane mode **3**. As summarized in Table 2, mode **3** is present in all three systems so that directed phonon propagation along the nanopores can be regarded as a generic feature of elastic impedance contrast nanocomposites consisting of AAO and a fluid infiltrated into the nanopores. Strikingly, the experimentally determined and the simulated longitudinal sound velocities along the nanopores associated with mode **3** are in good agreement with the bulk sound velocities of the corresponding liquids (*cf.* Table 1 and Table 2). The experimental value of c_l belonging to mode **3** in the system AAO/liquid PVDF could not be determined with high accuracy because of the damping of mode **3**, as discussed above.

Interestingly the interphase-sensitive in-plane flat band **2** is absent in the experimental in-plane band diagram of AAO/liquid PVDF (Figure 4b). We speculate that this outcome could have at least one of the following origins. (i) Owing to the nonpolar nature of PVDF, the absence of hydrogen bonds, and the high temperature of 453 K at which the BLS spectra were taken, no solidlike interphase is present. (ii) Only a thin, rudimentary solidlike interphase is present so that branch **2** is shifted to high frequencies outside the range considered here. (iii) Phonon damping reduces the conspicuity of branch **2**. (iv) Since liquid PVDF already has a high density, the density contrast between the PVDF in the vicinity of the pore walls and in the interior of the pores might be negligible so that the strength of branch **2** is significantly reduced.

As obvious from experimental dispersion diagrams or the corresponding simulations, all three systems consisting of AAO and an infiltrated fluid considered here, AAO/PDMS, AAO/PEG, and AAO/liquid PVDF, show bending of acoustic in-plane branch **1** indicative of in-plane mode localization as well as directed sound propagation along the nanopores through the fluid cylinders represented by acoustic out-of-plane branch **3**. The absence of interphase-sensitive in-plane flat mode **2** in the dispersion diagrams of the system AAO/liquid PVDF might be rationalized by the chemical nature of the PVDF or the elevated temperatures at which BLS measurements were carried out. However, it is remarkable that all the generic features of AAO-based nanocomposites containing liquids in the nanopores vanish when the liquid is solidified, as demonstrated by crystallization of the PVDF inside the nanopores. However, the highest acoustic out-of-plane branch **5** is virtually not affected by the nature of the material residing in the nanopores and is present not only in the dispersion diagrams of the systems AAO/PDMS, AAO/PEG, and AAO/

liquid PVDF but also in that of the system AAO/solid PVDF. Also, the longitudinal sound velocities belonging to mode **5** lie in the range from 6800 to 7200 m/s and are, therefore, similar to the longitudinal sound velocity of AAO before infiltration (Table 1). As previously demonstrated,[25] mode **5** mode is essentially confined to the AAO scaffold. Hence, the mechanical anisotropy $\sim c_5^2/c_1^2$ decreases with increasing ΔZ.

CONCLUSIONS

The hypersonic properties of elastic impedance contrast nanocomposites containing self-ordered AAO as inorganic model component, which exhibit well-defined periodicity and anisotropy, were studied by Brillouin light scattering spectroscopy. The hypersonic dispersion relations of the AAO/polymer nanocomposites can be tuned by adjusting elastic impedance contrast and density contrast between the AAO and the soft materials located in the nanopores. Peculiar features of AAO/polymer nanocomposites, such as phonon localization and anisotropic sound propagation, are most pronounced if both elastic impedance contrast and density contrast are high. The systems AAO/PEG and AAO/PDMS are characterized by the occurrence of an interphase-sensitive in-plane mode **2** in their band diagrams. However, mode **2** could not be detected in the case of the system AAO/liquid PVDF.

AAO-based hypersonic systems are not only mechanically and thermally stable but also transparent for visible light. Hence, in contrast to sonic crystals with macroscopic feature sizes, nanostructured AAO-based hypersonic systems enable well controlled and energy-efficient induction of phase transitions and other types of structural transformations to modify hypersonic band structures. As example in case, mode switching and modification of the phononic band structure by melting and crystallization of PVDF in AAO was demonstrated. Therefore, AAO has great potential as a platform for the design of tunable and switchable hypersonic phononic systems with engineered high-frequency acoustic properties. Recent progress in the fabrication of three-dimensional AAO architectures[48] might pave the way for the design of phononic device configurations operated in the GHz frequency range for mechanical filtering, advanced heat management, acousto-optical switching, and for unconventional sensor configurations. The design of membrane-based phononic device components based on AAO is straightforward, and the application of lithographic top-down techniques might yield hierarchical hypersonic architectures, which could be used as hypersonic waveguides and mode coupling components.

METHODS

Materials. PDMS with a weight-average molecular weight of 1350 g/mol and trimethylsilane end groups was synthesized by anionic polymerization under vacuum. To this end, 20 g of trimethylcyclotrisiloxane monomer was dissolved in a mixture of 53 mL of tetrahydrofuran and 41 mL of cyclohexane. The solvents were dried with a mixture of diphenylethene and an excess of butyllithium. The polymerization was initiated by adding 1.4 mol *sec*-butyllithium in hexane at room temperature and then quenched by the addition of an excess of trimethylchlorosilane after a reaction time of 4 h. PEG with a weight-average molecular weight of 400 g/mol and hydroxyl end groups was synthesized by anionic polymerization under vacuum. *sec*-Butyllithium was added to a solution of 20 g of ethylene oxide in 200 g of THF. After a reaction time of 12 h, the polymerization was quenched by methanol. Molecular weights were determined by gel permeation chromatography (GPC) against PEO standards using dimethylformamide as solvent. PVDF with a weight average molecular weight of 180 000 g/mol and a number-average molecular weight of 71 000 g/mol was purchased from Aldrich and used as received.

Preparation and Infiltration of Self-Ordered AAO. Self-ordered AAO was prepared following Masuda's two step anodization process.[18,19] Briefly, ultrapure aluminum substrates (99.999%) were electropolished in a 1:4 mixture of $HClO_4$ and absolute ethanol before anodization in 0.3 M oxalic acid at 40 V. Thus, AAO with a lattice constant of 100 nm, a pore diameter of 35 nm and a pore depth of 20 μm was obtained. To increase the porosities, the nanopores were widened to 60 nm by isotropic etching in 0.3 M oxalic acid at 30 °C. The underlying aluminum substrate was etched with a mixture of 1.7 g of $CuCl \cdot 2H_2O$, 50 mL of concentrated HCl and 50 mL of deionized water. PDMS and PEG were then infiltrated into the AAO at room temperature. Both the PDMS and the PEG used here had low molecular weights far below the critical molecular weight for the occurrence of entanglements.[49] Because of their oligomeric rather than polymeric character, both materials readily infiltrated the AAO, presumably according to the snap-off mechanism.[23,50] PVDF was infiltrated at 200 °C for 10 min. Depending on the experimental conditions, PVDF precursor films can wet the pore walls of AAO, or PVDF can infiltrate AAO according to classical capillarity.[23] Here, the diameter of the pores in the AAO approached the characteristic dimensions of the macromolecules so that, in any case, the pore volume was completely filled with polymer. The AAO containing PVDF was cooled to room temperature at a cooling rate of 1 K/min in the presence of a bulk PVDF film on the surface of the AAO, which was removed prior to BLS measurements. The Maxwell-Garnett theory was used to calculate effective refractive indices of the nanocomposites thus obtained as follows: $(\varepsilon_{eff} - \varepsilon_{alumina})/(\varepsilon_{eff} + 2\varepsilon_{alumina}) = f \times (\varepsilon_{pore} - \varepsilon_{alumina})/(\varepsilon_{pore} + 2\varepsilon_{alumina})$. ε_{eff}, $\varepsilon_{alumina}$, and ε_{pore} denote the refractive indices of the effective medium, alumina, and the material contained in the nanopores, respectively. Refractive indices of 1.41, 1.45, and 1.42 were used for PDMS, PEG, and PVDF, respectively, and a refractive index of 1.65[51] was used for AAO.

BLS Spectroscopy. Brillouin light scattering measurements were conducted with a Tandem Fabry–Perot Interferometer (JRS Scientific Instruments). The BLS measurements on AAO/PEG samples were carried out in the presence of a bulk PEG film on the surface of the AAO. In the case of the AAO/PDMS samples and the AAO/PVDF samples the PDMS and PVDF surface films were removed with blades prior to the BLS measurements.

Acknowledgment. We thank T. Wagner (MPI for Polymer Research) for synthesizing poly(dimethly siloxane) and polyethylene glycol, as well as S. Kallaus and K. Sklarek (MPI of Microstructure Physics) for the preparation of AAO. Funding by the German Research Foundation (Priority Program 1369 and JO 370/2-1) is gratefully acknowledged. Y. Pennec and B. Djafari-Rouhani acknowledge "Le Conseil Regional Nord-Pas de Calais" for financial support.

Supporting Information Available: Differential scanning calorimetry of bulk PVDF and PVDF nanostructures in AAO and complete theoretical phononoic dispersion relations for in-plane and out-of-plane propagation in both liquid and solid PVDF-filled AAO. This material is available free of charge via the Internet at http://pubs.acs.org.

REFERENCES AND NOTES

1. Yang, S. X.; Page, J. H.; Liu, Z. Y.; Cowan, M. L.; Chan, C. T.; Sheng, P. Ultrasound Tunneling through 3D Phononic Crystals. *Phys. Rev. Lett.* **2002**, *88*, 104301.
2. Yang, S. X.; Page, J. H.; Liu, Z. Y.; Cowan, M. L.; Chan, C. T.; Sheng, P. Focusing of Sound in a 3D Phononic Crystal. *Phys. Rev. Lett.* **2004**, *93*, 024301.
3. Kent, A. J.; Kini, R. N.; Stanton, N. M.; Henini, M.; Glavin, B. A.; Kochelap, V. A.; Linnik, T. L. Acoustic Phonon Emission from a Weakly Coupled Superlattice under Vertical Electron Transport: Observation of Phonon Resonance. *Phys. Rev. Lett.* **2006**, *96*, 215504.
4. Lu, M. H.; Zhang, C.; Feng, L.; Zhao, J.; Chen, Y. F.; Mao, Y. W.; Zi, J.; Zhu, Y. Y.; Zhu, S. N.; Ming, N. B. Negative Birefraction of Acoustic Waves in a Sonic Crystal. *Nat. Mater.* **2007**, *6*, 744–748.
5. Lu, M. H.; Liu, X. K.; Feng, L.; Li, J.; Huang, C. P.; Chen, Y. F.; Zhu, Y. Y.; Zhu, S. N.; Ming, N. B. Extraordinary Acoustic Transmission through a 1D Grating with Very Narrow Apertures. *Phys. Rev. Lett.* **2007**, *99*, 174301.
6. Christensen, J.; Fernandez-Dominguez, A. I.; De Leon-Perez, F.; Martin-Moreno, L.; Garcia-Vidal, F. J. Collimation of Sound Assisted by Acoustic Surface Waves. *Nat. Phys.* **2007**, *3*, 851–852.
7. Martinezsala, R.; Sancho, J.; Sanchez, J. V.; Gomez, V.; Llinares, J.; Meseguer, F. Sound-Attenuation by Sculpture. *Nature* **1995**, *378*, 241.
8. de Espinosa, F. R. M.; Jimenez, E.; Torres, M. Ultrasonic Band Gap in a Periodic Two-Dimensional Composite. *Phys. Rev. Lett.* **1998**, *80*, 1208–1211.
9. Liu, Z. Y.; Zhang, X. X.; Mao, Y. W.; Zhu, Y. Y.; Yang, Z. Y.; Chan, C. T.; Sheng, P. Locally Resonant Sonic Materials. *Science* **2000**, *289*, 1734–1736.
10. Vasseur, J. O.; Deymier, P. A.; Chenni, B.; Djafari-Rouhani, B.; Dobrzynski, L.; Prevost, D. Experimental and Theoretical Evidence for the Existence of Absolute Acoustic Band Gaps in Two-Dimensional Solid Phononic Crystals. *Phys. Rev. Lett.* **2001**, *86*, 3012–3015.
11. Page, J. H.; Sheng, P.; Schriemer, H. P.; Jones, I.; Jing, X. D.; Weitz, D. A. Group Velocity in Strongly Scattering Media. *Science* **1996**, *271*, 634–637.
12. Pennec, Y.; Djafari-Rouhani, B.; Vasseur, J. O.; Khelif, A.; Deymier, P. A. Tunable Filtering and Demultiplexing in Phononic Crystals with Hollow Cylinders. *Phys. Rev. E* **2004**, *69*, 046608.
13. Cheng, W.; Wang, J. J.; Jonas, U.; Fytas, G.; Stefanou, N. Observation and Tuning of Hypersonic Bandgaps in Colloidal Crystals. *Nat. Mater.* **2006**, *5*, 830–836.
14. Gorishnyy, T.; Jang, J. H.; Koh, C.; Thomas, E. L. Direct Observation of a Hypersonic Band Gap in Two-Dimensional Single Crystalline Phononic Structures. *Appl. Phys. Lett.* **2007**, *91*, 121915.
15. Baumgartl, J.; Zvyagolskaya, M.; Bechinger, C. Tailoring of Phononic Band Structures in Colloidal Crystals. *Phys. Rev. Lett.* **2007**, *99*, 205503.
16. Still, T.; Cheng, W.; Retsch, M.; Sainidou, R.; Wang, J.; Jonas, U.; Stefanou, N.; Fytas, G. Simultaneous Occurrence of Structure-Directed and Particle-Resonance-Induced Phononic Gaps in Colloidal Films. *Phys. Rev. Lett.* **2008**, *100*, 194301.
17. Wang, L.; Li, B. Phononics Gets Hot. *Phys. World* **2008**, *21*, 27–29.
18. Masuda, H.; Fukuda, K. Ordered Metal Nanohole Arrays Made by a 2-Step Replication of Honeycomb Structures of Anodic Alumina. *Science* **1995**, *268*, 1466–1468.
19. Masuda, H.; Hasegwa, F.; Ono, S. Self-Ordering of Cell Arrangement of Anodic Porous Alumina Formed in Sulfuric Acid Solution. *J. Electrochem. Soc.* **1997**, *144*, L127–L130.
20. Sulka, G. D. Highly Ordered Anodic Porous Alumina Formation by Self-Organized Anodizing. In *Nanostructured Materials in Electrochemistry*; Eftekhari, A., Ed.; Wiley-VCH: Weinheim, Germany, 2008.
21. Martin, C. R. Template Synthesis of Polymeric and Metal Microtubules. *Adv. Mater.* **1991**, *3*, 457–459.
22. Martin, C. R. Nanomaterials—A Membrane-Based Synthetic Approach. *Science* **1994**, *266*, 1961–1966.
23. Steinhart, M. Supramolecular Organization of Polymeric Materials in Nanoporous Hard Templates. *Adv. Polym. Sci.* **2008**, *220*, 123–187.
24. Steinhart, M.; Zimmermann, S.; Goring, P.; Schaper, A. K.; Gösele, U.; Weder, C.; Wendorff, J. H. Liquid Crystalline Nanowires in Porous Alumina: Geometric Confinement *versus* Influence of Pore Walls. *Nano Lett.* **2005**, *5*, 429–434.
25. Sato, A.; Knoll, W.; Pennec, Y.; Djafari-Rouhani, B.; Fytas, G.; Steinhart, M. Anisotropic Propagation and Confinement of High Frequency Phonons in Nanocomposites. *J. Chem. Phys.* **2009**, *130*, 111102.
26. Shimazaki, Y.; Hojo, F.; Takezawa, Y. Highly Thermoconductive Polymer Nanocomposite with a Nanoporous α-Alumina Sheet. *ACS Appl. Mater. Interfaces* **2009**, *1*, 225–227.
27. Penciu, R. S.; Kriegs, H.; Petekidis, G.; Fytas, G.; Economou, E. N. Phonons in Colloidal Systems. *J. Chem. Phys.* **2003**, *118*, 5224–5240.
28. Shih, H.; Flory, P. J. Equation-of-State Parameters for Poly(dimethylsiloxane). *Macromolecules* **1972**, *5*, 758–761.
29. Orwoll, R. A. Densities, Coefficients of Thermal Expansion, and Compressibilities of Amorphous Polymers. In *Physical Properties of Polymers Handbook*; Mark, J. E., Ed.; Springer: New York, 2006.
30. Mekhilef, N. Viscoelastic and Pressure-Volume-Temperature Properties of Poly(vinylidene fluoride) and Poly(vinylidene fluoride)-Hexafluoropropylene Copolymers. *J. Appl. Polym. Sci.* **2001**, *80*, 230–241.
31. Miller, R. L. Solid State Properties. In *Polymer Handbook*, 4th ed.; Brandrup, J.; Immergut, E. H.; Grulke, E. A., Eds.; John Wiley & Sons: New York, 1999.
32. Hartmann, B.; Jarzynsk, J. Immersion Apparatus for Ultrasonic Measurements in Polymers. *J. Acoust. Soc. Am.* **1974**, *56*, 469–1477.
33. Litvinov, V. M.; Spiess, H. W. ^{2}H NMR-Study of Molecular Motions in Polydimethylsiloxane and Its Mixtures with Aerosils. *Makromol. Chem.* **1991**, *192*, 3005–3019.
34. Cosgrove, T.; Turner, M. J.; Thomas, D. R. The Adsorption of Polydimethylsiloxane onto Silica from the Melt. *Polymer* **1997**, *38*, 3885–3892.
35. Kirst, K. U.; Kremer, F.; Litvinov, V. M. Broad—Band Dielectric-Spectroscopy on the Molecular-Dynamics of Bulk and Adsorbed Poly(dimethylsiloxane). *Macromolecules* **1993**, *26*, 975–980.
36. Tsagaropoulos, G.; Eisenberg, A. Dynamic-Mechanical Study of the Factors Affecting the 2 Glass-Transition Behavior of Filled Polymers—Similarities and Differences with Random Ionomers. *Macromolecules* **1995**, *28*, 6067–6077.
37. Arrighi, V.; Higgins, J. S.; Burgess, A. H.; Floudas, G. Local Dynamics of Poly(dimethyl siloxane) in the Presence of Reinforcing Filler Particles. *Polymer* **1998**, *39*, 6369–6376.
38. Evmenenko, G.; Mo, H. D.; Kewalramani, S.; Dutta, P. Conformational Rearrangements in Interfacial Region of Polydimethylsiloxane Melt Films. *Polymer* **2006**, *47*, 878–882.
39. Horn, R. G.; Israelachvili, J. N. Molecular-Organization and Viscosity of a Thin-Film of Molten Polymer between Two Surfaces as Probed by Force Measurements. *Macromolecules* **1988**, *21*, 2836–2841.
40. Evmenenko, G.; Dugan, S. W.; Kmetko, J.; Dutta, P. Molecular Ordering in Thin Liquid Films of Polydimethylsiloxanes. *Langmuir* **2001**, *17*, 4021–4024.
41. Primak, S. V.; Jin, T.; Dagger, A. C.; Finotello, D.; Mann, E. K.

Chain Segment Order in Ultrathin Polymer Films: A Deuterium NMR Study. *Phys. Rev. E* **2002**, *65*, 031804.
42. Jagadeesh, B.; Demco, D. E.; Blümich, B. Surface Induced Order and Dynamic Heterogeneity in Ultra Thin Polymer Films: A ^{1}H Multiple-Quantum NMR Study. *Chem. Phys. Lett.* **2004**, *393*, 416–420.
43. Lovinger, A. J. Ferroelectric Polymers. *Science* **1983**, *220*, 1115–1121.
44. Hasegawa, R.; Takahash, Y.; Tadokoro, H.; Chatani, Y. Crystal-Structures of Three Crystalline Forms of Poly(vinylidene fluoride). *Polym. J.* **1972**, *3*, 600–610.
45. Steinhart, M.; Senz, S.; Wehrspohn, R. B.; Gösele, U.; Wendorff, J. H. Curvature-Directed Crystallization of Poly(vinylidene difluoride) in Nanotube Walls. *Macromolecules* **2003**, *36*, 3646–3651.
46. Steinhart, M.; Goring, P.; Dernaika, H.; Prabhukaran, M.; Gösele, U.; Hempel, E.; Thurn-Albrecht, T. Coherent Kinetic Control over Crystal Orientation in Macroscopic Ensembles of Polymer Nanorods and Nanotubes. *Phys. Rev. Lett.* **2006**, *97*, 027801.
47. Martin, J.; Mijangos, C.; Sanz, A.; Ezquerra, T. A.; Nogales, A. Segmental Dynamics of Semicrystalline Poly(vinylidene fluoride) Nanorods. *Macromolecules* **2009**, *42*, 5395–5401.
48. Lee, W.; Schwirn, K.; Steinhart, M.; Pippel, E.; Scholz, R.; Gösele, U. Structural Engineering of Nanoporous Anodic Aluminium Oxide by Pulse Anodization of Aluminium. *Nat. Nanotechnol.* **2008**, *3*, 234–239.
49. Fetters, L. J.; Lohse, D. J.; Milner, S. T.; Graessley, W. W. Packing Length Influence in Linear Polymer Melts on the Entanglement, Critical, and Reptation Molecular Weights. *Macromolecules* **1999**, *32*, 6847–6851.
50. Lenormand, R. Liquids in Porous-Media. *J. Phys.: Condens. Matter* **1990**, *2*, Sa79–Sa88.
51. Choi, J.; Luo, Y.; Wehrspohn, R. B.; Hillebrand, R.; Schilling, J.; Gosele, U. Perfect Two-Dimensional Porous Alumina Photonic Crystals with Duplex Oxide Layers. *J. Appl. Phys.* **2003**, *94*, 4757–4762.